Simulation of self-assembled nanopatterns in strained 2D alloys on the face centered cubic (111) surface

2008 J. Phys.: Condens. Matter 20 265004

(http://iopscience.iop.org/0953-8984/20/26/265004)

J. Phys.: Condens. Matter **20** (2008) 265004 (7pp) doi:10.1088/0953-8984/20/26/265004

Simulation of self-assembled nanopatterns in strained 2D alloys on the face centered cubic (111) surface

S Weber[1], M Biehl[2], M Kotrla[3] and W Kinzel[1]

[1] Institut für Theoretische Physik und Astrophysik, Universität Würzburg, Am Hubland, 97074 Würzburg, Germany
[2] Institute for Mathematics and Computing Science, University of Groningen, PO Box 407, 9700 AK Groningen, The Netherlands
[3] Institute of Physics, Academy of Sciences of the Czech Republic, Na Slovance 2, 182 21 Prague 8, Czech Republic

Received 18 February 2008, in final form 25 April 2008
Published 22 May 2008
Online at stacks.iop.org/JPhysCM/20/265004

Abstract
We investigate the formation of nanostructures in 2D strained alloys on face centered cubic (111) surfaces by means of equilibrium Monte Carlo simulations. In the framework of an off-lattice model, we consider one monolayer of two bulk-immiscible adsorbates A and B with negative and positive misfit relative to the substrate, respectively. Simulations show that the adsorbates partly self-organize into island or stripe-like patterns. We show how these structures depend on the relative misfits, interaction, and concentration of components. The morphology is quite different for phase separation and intermixing regimes.

1. Introduction

Today, many applications of components based on nanostructures are emerging, among others e.g. quantum dots [1]. In order to further advance this field, and routinely produce nanocomponents, a thorough understanding of mechanisms governing the formation of nanostructures is required. The key process of formation of nanostructures is self-organization. Self-organization of quantum dots has been investigated using continuum theory; see e.g. [2]. However, understanding of microscopic processes that are relevant for the formation of nanostructured surfaces is important for the development of novel electronic and magnetic devices. In this paper, we adopt this view.

In metal epitaxy, the formation of surface alloys is of particular interest. Often, elements which are bulk-immiscible form alloys in a single atomic layer on the surface; see [3] and references therein. A particularly interesting effect is the formation of two-dimensional self-assembled ordered arrays of dots, so-called droplets, or alternating rows of domains, i.e. stripes [4–6]. Multi-component materials are of great interest because they provide the possibility of preparing new systems with unique properties. For example, self-assembled lateral multilayers are found to exhibit a significant anisotropic magnetoresistance [7]. On the other hand, it has also been observed that instabilities can lead to dendritic growth [8], thus reducing the applicability of the complex material.

Recently, we have evaluated the influence of two competing mechanisms, strain relaxation and kinetic segregation, on island growth in a ternary system of two adsorbates with opposite misfit relative to the substrate [9]. In particular, we have discussed the problem of island ramification observed in [8] for CoAg/Ru(0001). However, we considered only a simplified model for simple cubic lattices.

In this paper, our focus is on pattern formation in metal heteroepitaxy of two chemically different adsorbates which form a thin alloy film on a given substrate. We study equilibrium properties of two materials which we denote as A and B, deposited on a suitable substrate S. We consider an fcc(111) surface and investigate the morphology of a thin alloy film depending on the misfit, inter-species interactions, and concentration of components.

The problem of patterns in surface alloys has been previously studied by different methods. For instance, Ozoliņš *et al* employed hybrid atomistic–continuum models [10]. Ng and Vanderbilt's investigation of the formation of periodic domains is based on continuum elasticity theory [11]. Clearly, the applicability of macroscopic approaches on the nanoscale is limited. Here we aim at the development of a relatively simple approach, which facilitates a microscopic treatment that can

be applied over a broad range of alloy systems. Simulations of the model described below allow us to explore the specific influence of external conditions and microscopic parameters on specific properties of equilibrium patterns.

2. Model and methods

Computer simulations of homoepitaxial growth are often based on discrete solid-on-solid models in which particles can only move from one pre-defined binding site to another one with rates controlled by diffusion barriers, or by variable parameters [12]. In heteroepitaxy, adsorbate and substrate lattice constants differ, and substantial strain is usually generated. In order to describe effects of strain, a modified approach is needed. A simple approximative way to proceed is to modify the diffusion barriers via a dependence on the lattice mismatch as e.g. in [13]. In a more realistic approach, one should replace discrete models with pre-defined lattices using a continuous approach in which contributions of elastic energy to the total energy of the sample are considered. See e.g. [14, 15] for an overview and discussion.

Here, we employ an off-lattice model which allows for continuous particle positions. The atomistic structure now naturally emerges from the symmetry of the particle interactions used, and the symmetry of the substrate. This type of model has been employed in previous investigations of heteroepitaxial growth, at first in the simpler 1 + 1-dimensional case, for instance in the context of strain relief through misfit dislocations [16–19] or the so-called Stranski–Krastanov growth mode [20]. The method was applied, also to 2 + 1-dimensional systems, for the study of the effect of strain on diffusion barriers in [21], however, for a simple cubic lattice. Recently for the same lattice, a mixed adsorbate system was studied in [9] and some aspects of the stability of nanostructured alloy formation were explored.

We model a ternary system of adsorbate metals A, B and substrate S. In order to keep the number of model parameters small and to facilitate simulations at reasonable computational cost, we consider fairly simple pairwise interactions. In the following, U_{pq} describes the potential energy contribution of two interacting particles where the subscripts $p, q \in \{\mathrm{A}, \mathrm{B}, \mathrm{S}\}$ specify which elements are involved.

We consider as a simple choice the Lennard-Jones potential [22]

$$U_{pq}(r) = E_{pq}\left[\left(\frac{\sigma_{pq}}{r}\right)^{12} - \left(\frac{\sigma_{pq}}{r}\right)^{6}\right]. \tag{1}$$

Here, r is the distance of the two particles and the prefactor E_{pq} controls the depth of the potential, while the parameter σ_{pq} determines the equilibrium distance of two isolated particles $r^0_{pq} = 2^{1/6}\sigma_{pq}$. Hence, the lattice constant in an undisturbed monatomic system of, say, element p would be directly proportional to σ_{pp}.

In this work, we do not aim at material specific simulations; our goal is a qualitative understanding of mechanisms that govern two-dimensional alloy formation in a ternary system. We choose the values of parameters $\{E_{pq}, \sigma_{pq}\}$ and the mismatch to represent several illustrative situations, and we study the dependence of essential features of the pattern formation on the values of the model parameters. In the following, we use the briefer notation $E_q = E_{qq}$, $\sigma_q = \sigma_{qq}$. Hence, e.g., the interaction strength within the substrate is denoted by E_S. The parameter $\sigma_{\mathrm{SS}} = \sigma_\mathrm{S}$ defines the unit of length in the following, i.e. $\sigma_\mathrm{S} = 1$. Our model, as formulated so far, allows us to treat different physical situations. In order to present results for illustrative situations, we shall choose particular values of some model parameters. With respect to the misfit relative to the substrate, we study symmetric configurations with

$$\sigma_\mathrm{A} = 1 - \varepsilon \qquad \text{and} \qquad \sigma_\mathrm{B} = 1 + \varepsilon \quad (\varepsilon > 0) \tag{2}$$

for the two adsorbates. In the general case, mutual interactions of adatoms of different type, that is the parameters E_A and E_B, are different, and also the interactions of particles of type A or B with the substrate are different. However, we choose here for the simplification equal energies $E_\mathrm{A} = E_\mathrm{B}$ and fix their magnitude relative to E_S:

$$E_\mathrm{A} = E_\mathrm{B} = E_\mathrm{S}/6. \tag{3}$$

Another simplification is that due to the relatively strong interaction E_S, diffusion hops of substrate particles and interdiffusion of the substrate and adsorbate can be neglected.

Furthermore, in order to keep the number of free parameters small, we follow a standard approach and set for interactions involving different metals in the following way:

$$E_{pq} = \sqrt{E_p E_q} \qquad \text{and} \qquad \sigma_{pq} = (\sigma_p + \sigma_q)/2 \qquad \text{where } p, q \in \{\mathrm{A}, \mathrm{B}, \mathrm{S}\}. \tag{4}$$

Note that as a result of our choice in the equation (3), the interactions of different atom types with the substrate are the same. In this paper, we do not study the effect of different diffusion barriers for adatoms on the substrate. Instead, we focus on the effect of interaction between different particle types, which exerts the mainly control on the patterns obtained. The relation (4) is used in all cases except for determination of E_AB; this parameter is varied independently. It is motivated by the focus on the effect of interaction between different particle types.

In the simulation, seven layers of the substrate fcc crystal are prepared, displaying a single (111) surface. Throughout the following, we consider hexagonal substrate cells with a side length of 51 particles, reflecting the symmetry of the lattice. The positions of all particles in the bottom three layers are kept fixed throughout the simulations in order to stabilize the crystal structure. The (111) surface is covered by a single layer of adsorbate which contains a random mixture of A and B particles. The concentrations of elements are fixed and denoted as η_A and η_B with $\eta_\mathrm{A} + \eta_\mathrm{B} = 1$.

For the range of misfits ε considered here, we do not observe the formation of dislocations. Hence, the continuous spatial positions of all particles, including the adsorbate, are in the vicinity of sites in an undisturbed substrate lattice. At any given time, the precise location of all particles corresponds to a local minimum of the total potential energy in the system. In order to speed up the required calculations of

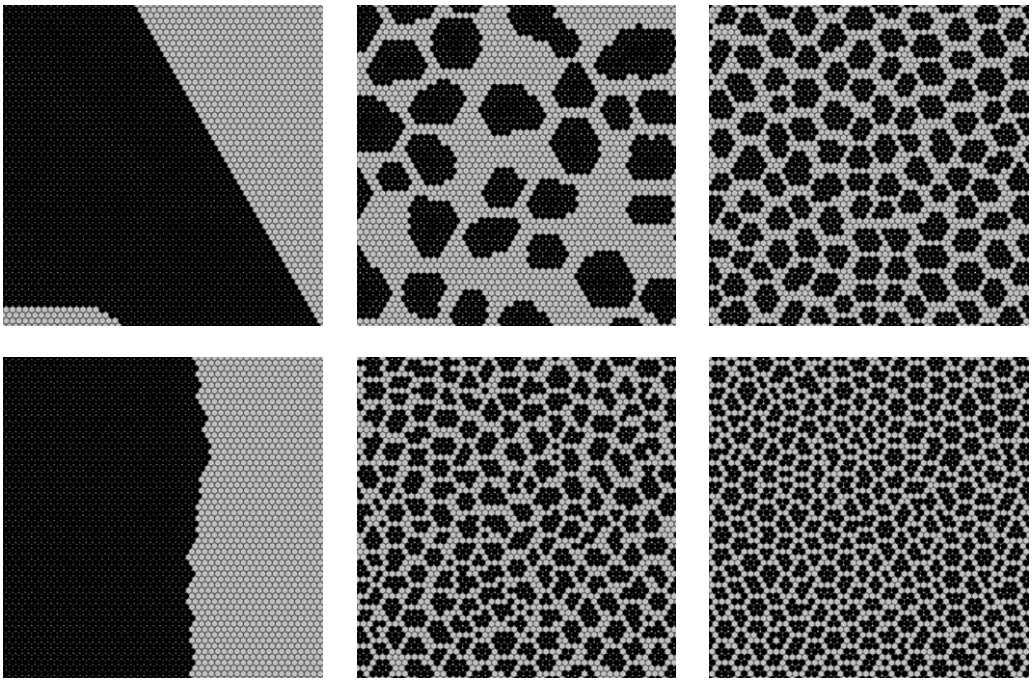

Figure 1. Upper row: simulation results for Lennard-Jones interactions with $E_{AB} = 0.35$ eV and $\varepsilon = 0\%, 5.5\%, 7.5\%$ (from left to right); the particle concentrations are $\eta_A = \eta_B = 0.5$. The panels show 50×50 sections; the bigger B particles are shown in black. Lower row: simulation results for $E_{AB} = 0.45$ eV; all other values as above.

potential energies, we cut off the Lennard-Jones interactions for distances larger than $r_{cut} = 3r^0_{SS}$.

The system is driven towards thermal equilibrium at temperature T by means of a rejection-free Monte Carlo method [23, 24]. Since the precise path towards equilibrium is of no interest here, we have implemented efficient dynamics, which need not have a realistic microscopic counterpart; however, it speeds up equilibration considerably. We consider the non-local exchange of one A and one B particle on the surface with no limitation on their distance. This yields a significantly faster equilibration than local Kawasaki dynamics [23].

The exchange is implemented as follows. Let us consider particle A at site i, and particle B at site j. In every MC step, the pair is selected according to the rates

$$r_{i\to j} = \mathrm{e}^{\frac{\Delta H_i - \Delta H_j}{2kT}} \tag{5}$$

which satisfy the detailed balance condition. Here, $\Delta H_x = H_x(\mathrm{A}) - H_x(\mathrm{B})$ denotes the energy difference of the systems with an A and B particles at site x. In order to obtain, for instance, $H_x(\mathrm{A})$, an A particle is placed at the corresponding site and all particles within a distance r_{cut} are relaxed to positions which correspond to a local minimum of the total potential energy in the system. In order to avoid complications, an exchange process is only permitted if the distance between sites i and j is larger than r_{cut}.

Proper binding states correspond to local minima of the total potential energy with respect to the positions of all particles in the system. After exchanging two adsorbate atoms in the above described manner, it is necessary, in principle, to fine-tune all particle coordinates in order to ensure that the system resides precisely in such a local minimum. This can be achieved by employing gradient based relaxation techniques. For the sake of reducing computational costs, we apply this relaxation only to particles within a maximum distance r_{cut} from both of the exchanged adsorbate atoms. Hence, we take advantage of the effective cut-off of the Lennard-Jones interaction at large distances, once more. Clearly, this simplification can lead to inaccuracies. In order to prevent them from accumulating over long simulation runs, we perform a proper relaxation of the entire system after a given number of MC steps (here 10^4).

3. Results

Our simulations show that the misfit has, as expected, a strong effect on the structure of the surface alloy. Figure 1, upper row, shows a series of surface snapshots after 10^5 MC steps with different values of ε; the energies are $E_S = 3$ eV, $E_A = E_B = 0.5$ eV, $E_{AB} = 0.35$ eV, and the temperature T is set to 250 K and interactions are given by the 12, 6 Lennard-Jones potential in (1).

Figure 1 shows results for adsorbate concentrations $\eta_A = \eta_B = 0.5$; the smaller A particles with negative misfit are drawn in gray and B particles with positive misfit in black.

In the case of zero misfit, $\varepsilon = 0$, the two different adsorbates are completely separated into two regions, thus minimizing the number of A/B nearest neighbor pairs with unfavorable interaction energy E_{AB}. But with increasing misfit an increasing number of small islands are formed. The formation of large islands of B particles becomes increasingly unlikely as the conflict between the natural B–B spacing and

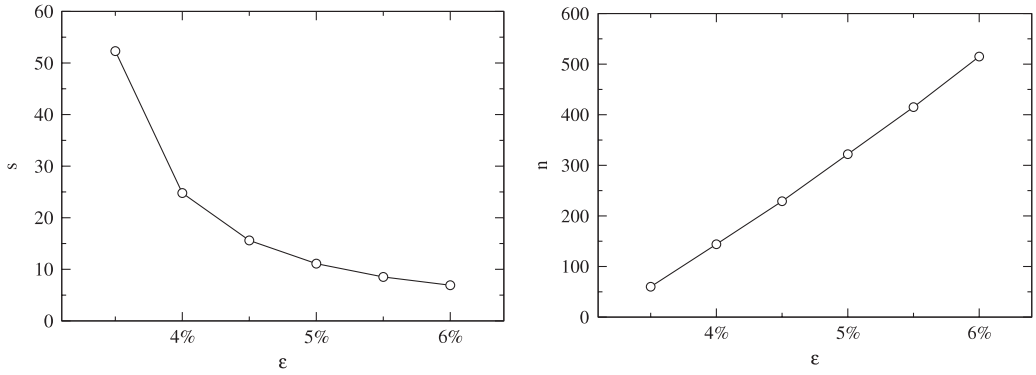

Figure 2. Left: the averaged size s of islands consisting of B particles versus the absolute value of the misfit ε at the energies $E_S = 3$ eV, $E_A = E_B = 0.5$ eV, $E_{AB} = 0.45$ eV and the particle concentrations $\eta_A = \eta_B = 0.5$. Right: the number of islands n versus the absolute value of the misfit ε at the same parameters.

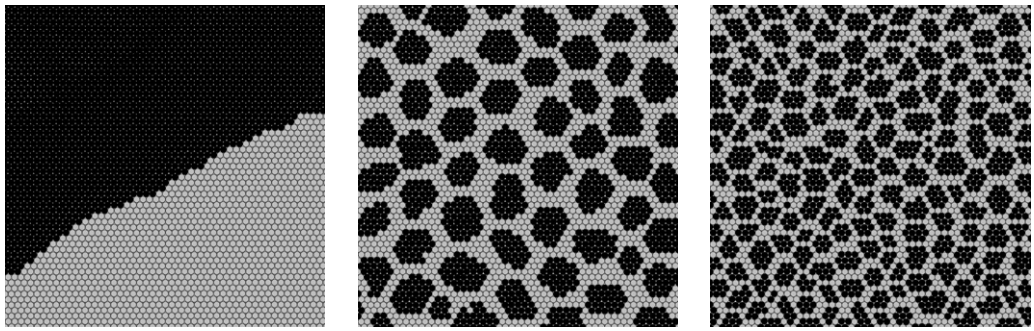

Figure 3. Surfaces in the model with a modified potential with exponents $n = 10.5$ and $m = 5.5$; equation (6). The parameters are $E_{AB} = 0.40$ eV, $\varepsilon = 0\%, 5.5\%, 7.5\%$ (from left to right), and $\eta_A = \eta_B = 0.5$.

the sites provided by the substrate would result in energetically unfavorable particle locations. As a consequence, B particles arrange in smaller clusters as the misfit increases.

Obviously, the interaction energy E_{AB} also influences the size of B islands. The smaller E_{AB}, the more energy it costs to realize boundaries between A and B domains and the larger the clusters will be; see figure 1 (lower row) for typical surface configurations with $E_{AB} = 0.45$ eV. An even larger interaction energy $E_{AB} > E_A, E_B$ would favor larger interfaces between the two types. While the average island size becomes smaller with increasing misfit, the number of islands in the system increases (figure 2) as the adsorbate concentrations η_A and η_B are fixed.

Potentials with exponents $n \neq 12$ and $m \neq 6$, in the form

$$U_{pq} = E_{pq}\left[\frac{m}{n-m}\left(\frac{r^o_{pq}}{r}\right)^n - \frac{n}{n-m}\left(\frac{r^o_{pq}}{r}\right)^m\right] \quad (6)$$

with $n > m$ [25], lead to very similar results to the Lennard-Jones potential with $n = 12, m = 6$, but the computational effort increases. As an example, figure 3 shows surfaces from simulations with $n = 10.5$ and $m = 5.5$. Our qualitative findings do not depend on the detailed properties of the potential considered, and we expect them to persist for a large variety of interactions.

The average island size changes also with the adatom concentrations η_A, η_B. Figure 4 displays a system with an A particle concentration of $\eta_A = 0.7$; the islands of B adatoms are slightly smaller than in the case of $\eta_A = \eta_B = 0.5$. In addition, the distance between B islands changes with $\frac{\eta_A}{\eta_B}$. As the diagram on the right-hand side indicates, small concentrations η_A lead to big B islands, because the B particles 'prefer' to form several big islands rather than many small islands. On increasing η_A, B islands become smaller and smaller, but for high values the averaged size depends only weakly on the concentration.

So far, we have considered the case $E_{AB} < E_A, E_B$. If the energy of interaction between the two adsorbates E_{AB} is larger than the interactions E_A, E_B, the situation changes and completely new structures emerge. In this case, we observe stripe-like structures, as shown in figure 5. Their form is affected by the misfit: large misfits lead to more bendings and fewer straight stripe sections, as a high misfit hinders the formation of long chains of particles.

In figure 6 the normalized distribution of the number of straight stripe lengths for miscellaneous misfits is plotted; it confirms the optical impression. The figure shows the frequency of straight parts of particle chains (sections without a bend), independent of the direction of these straight lines. Lower misfits result in more straight segments, in contrast to higher values. This effect originates from the fact that, for high positive misfits, particles which are jammed between two neighbors of the same type 'try' to sidestep and build a bend.

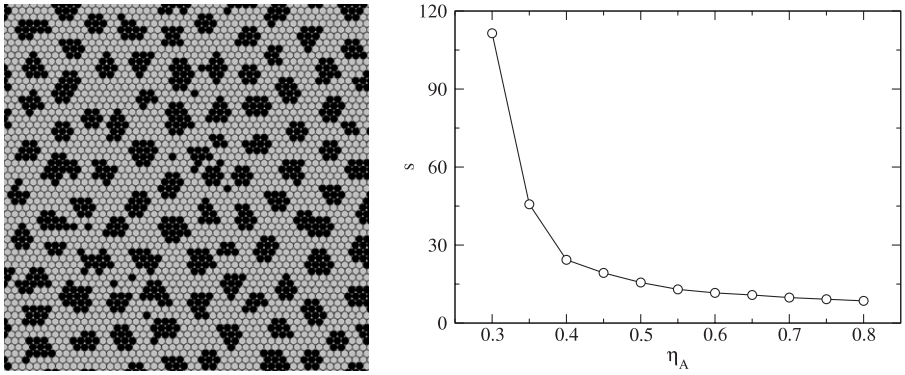

Figure 4. Left: simulation results for the Lennard-Jones potential with $E_S = 3$ eV, $E_A = E_B = 0.5$ eV, $E_{AB} = 0.45$ eV and $\varepsilon = 4.5\%$; the particle concentrations are set to $\eta_A = 0.7$ and $\eta_B = 0.3$. The panel shows a 50×50 section; the bigger B particles appear in black. Right: the averaged size s of islands consisting of B particles versus the concentration of the smaller A particles η_A.

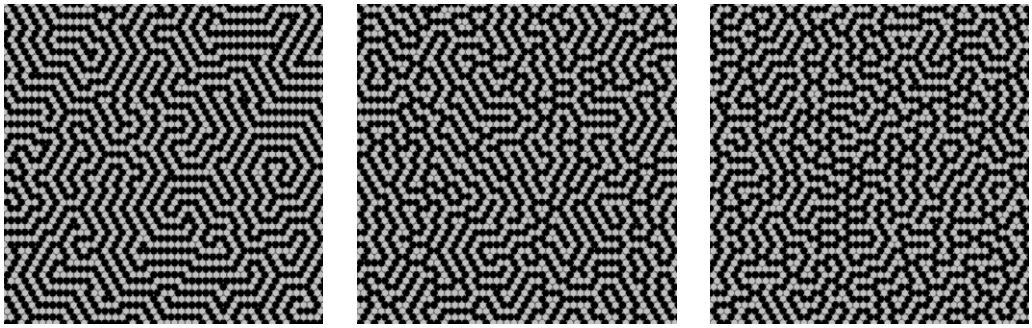

Figure 5. Surfaces observed for the Lennard-Jones potential with $E_S = 3$ eV, $E_A = E_B = 0.5$ eV, $E_{AB} = 1.50$ eV and $\varepsilon = 1.0\%, 4.0\%, 7.0\%$ (from left to right); the particle concentrations are $\eta_A = \eta_B = 0.5$. The panels show 50×50 sections; the bigger B particles appear in black.

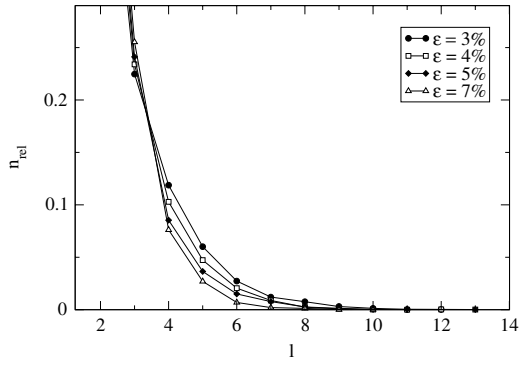

Figure 6. Relative number $n_{rel} = n/n_{\text{total}}$ of straight stripe lengths l in the system with Lennard-Jones interactions; parameters as in figure 5.

Hence, a meandering configuration has less strain and becomes more favorable for increasing misfit.

The variation of the particle concentration from a low to a high value leads to an interesting evolution of patterns. This is illustrated in figure 7, which shows the results of simulations for three different concentrations of B particles, energy $E_{AB} = 0.75$ eV, misfit of 1% and temperature $T = 250$ K. At low concentrations of the bigger B adatoms, each of them is surrounded by neighbors of A type only. For slightly larger η_B, short linear clusters of B atoms begin to form, and for $\eta_A \approx \eta_B$ we observe stripe formation throughout the system; cf figure 7 (center panel). Finally, a high concentration of B particles leads to the formation of patterns which are similar to those for the case of small η_B, but with the roles of A and B exchanged. In addition, one can recognize the formation of line defects in the right and left panels dominated by particles of different types.

4. Discussion

Our model allows systematic and relatively fast studies of equilibrium patterns in strained alloys and the dependence of their features on physical parameters. In order to draw correct conclusions, it is important to know whether the observed configurations are close to equilibrium. We aim at achieving equilibrated configurations by employing the non-local updating procedure and by performing a sufficient number of simulation steps. An important question in this context is how many MC steps are required to achieve this goal. To this end, we have inspected properties of the surface in the course of the on-going simulation. Figure 8 shows, as an example, the evolution of a system with $E_{AS} = 0.45$ eV and $\varepsilon = 4.5\%$ with increasing number of KMC steps. At the beginning, the adsorbate particles are arranged randomly, but for this set of model parameters, equilibrium is reached very fast and thereafter, only a few small changes affect the surface structures.

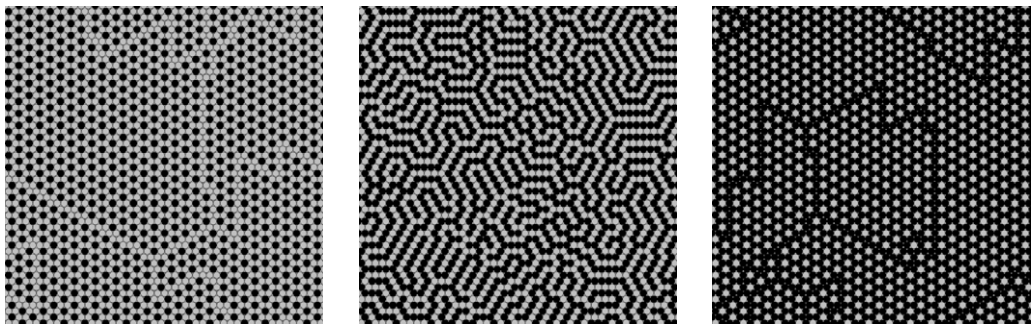

Figure 7. Simulation results for the Lennard-Jones potential with energies $E_S = 3$ eV, $E_A = E_B = 0.5$ eV, $E_{AB} = 0.75$ eV and misfit $\varepsilon = 1.0\%$; the concentrations of B particles are $\eta_B = 0.3, 0.5, 0.7$ (from left to right). The panels show 50×50 sections; the bigger B particles appear in black.

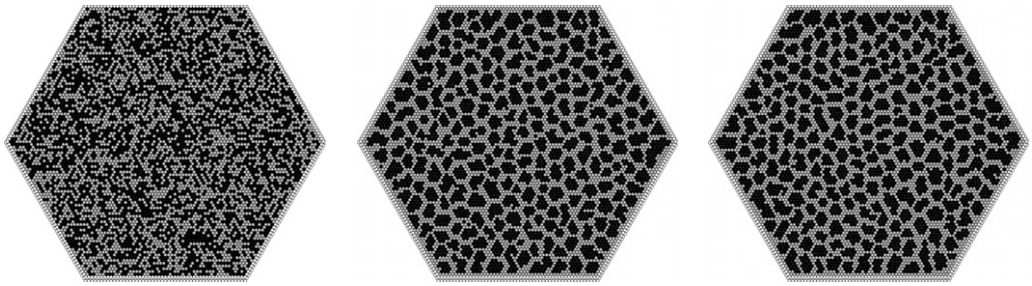

Figure 8. Simulation results for Lennard-Jones interactions with $E_S = 3.00$ eV, $E_A = 0.50$ eV, $E_{AB} = 0.45$ eV, and $\varepsilon = 4.5\%$: initial configuration and the configurations after 20×10^3 and after 140×10^3 MC steps (from left to right). The temperature is set to $T = 250$ K. The particles with positive misfit are drawn in black.

The optical impression is confirmed by the plots in figure 9. Already, after a few thousand steps, the average island size and the number of islands are both roughly constant and the graphs display only a few fluctuations. In the case of $E_{AS} = 0.35$ eV and $\varepsilon = 5.5\%$, which is also displayed in figure 9, the systems needs more steps to attain equilibrium. In the initial phase of the simulation, many steps are required to form the large islands typical for this set of parameters; however, after 100×10^3 MC steps the number of islands and their average size have become constant with almost no fluctuations due to the large island sizes. We investigated the dynamics of equilibration in more detail, and we found that the dependence of the size of islands consisting of B particles on the number of MC steps can be well fitted by a power law with the exponent approximately 0.2 in the example setting of $E_{AB} = 0.35$ eV and $\varepsilon = 5.5\%$.

In almost all our simulations the equilibrium is reached after at most 10^5 steps and the simulation can be stopped. However, in most cases the equilibrium had been reached even earlier.

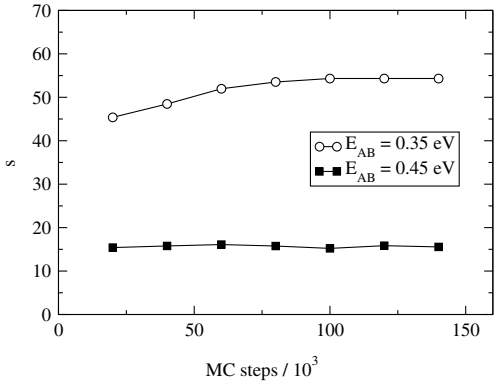

Figure 9. The average island size s of islands consisting of B particles versus the number of MC steps for $E_{AB} = 0.45$ eV, $\varepsilon = 4.5\%$ and $E_{AB} = 0.35$ eV, $\varepsilon = 5.5\%$.

5. Conclusions

In this paper, we have demonstrated that our off-lattice KMC model of a surface ternary system allows systematic and flexible investigation of equilibrium patterns in 2D strained alloys. In order to simulate the formation of structures, we use a rejection-free Monte Carlo method for the model in which the particles have continuous coordinates and adsorb heteroepitaxially at an fcc(111) surface. An interaction potential of the Lennard-Jones form is employed. Our model can be generalized to a multilayer situation. In this case we expect a richer set of possible surface patterns, as has been seen, for example, in Cu/Ru(0001) heteroepitaxy [26].

We have shown how equilibrium patterns change with misfit, energies of interaction between species, and concentration of components. We investigated two basically different situations: phase separation and a mixing regime.

In the case of $E_{AB} < E_A, E_B$, the adsorbed layer of A and B particles has the pattern formed by islands composed

from bigger B particles inserted inside a film of smaller A particles. The size of islands depends on the misfit ε and the interaction energy E_{AB}. The average size of islands decreases with increasing misfit and interaction energy. Higher values of both parameters lead to the formation of many small islands, in contrast to the case for smaller values, where only a few big islands are observed. The variation of the adatom concentrations changes the mean island size: at small concentrations of A particles the islands of B particles are quite big, and they become smaller and smaller with increasing concentration η_A. But for high η_A the averaged size depends only weakly on the concentration. This behavior is similar to the one observed for simple cubic lattices (cf figures 4 and 5 in [9]). It is furthermore robust against variation of the form of the interaction potential.

If E_{AB} is larger than E_A, E_B, stripes with a large interface between the two adsorbates arise. In this case the misfit affects the number of bendings and straight sections in these stripes. At low concentrations η_B we observe B islands surrounded by A particles. Intermediate concentrations result in the formation of stripes, while for large η_B an 'inverted' island pattern is observed with the roles of A and B exchanged. Qualitatively, the behavior resembles the evolution from 2D droplets to inverted 2D droplets as recently observed in self-assembled domain structures during deposition of Pb on Cu(111) [4, 5, 27].

Our model can be straightforwardly applied to the study of a variety of physical situations not elaborated in this paper, but characterized by different values of model parameters, for example, non-symmetric misfit, non-symmetric adsorbate–substrate interaction, or different adsorbate–adsorbate interactions.

It would be of interest to evaluate the applicability of the approach presented for studying alloy patterns on substrates with different lattice structure, e.g. fcc(110), or for calculation of phase diagrams as a function of adsorbate concentration or the temperature. The model can also be generalized to allow study of strained 3D alloys if inter-layer processes are included.

Acknowledgments

S Weber acknowledges support by the Deutsche Forschungsgemeinschaft. This work was also supported by joint funding under EU STRP 016447 MagDot and NSF DMR Award No. 0502737.

References

[1] Joyce B A, Kelires P C, Naumovets A G and Vvedensky D D (ed) 2005 *Quantum Dots: Fundamentals, Applications, and Frontiers* (*NATO Science Series II' Mathematics, Physics and Chemistry* vol 190) (New York: Springer)
[2] Golovin A A, Davis S H and Voorhees P W 2003 *Phys. Rev.* E **68** 056203
[3] Tersoff J 1995 *Phys. Rev. Lett.* **74** 434
[4] Plass R, Last J A, Bartelt N C and Kellog G L 2001 *Nature* **412** 875
[5] Plass R, Bartelt N C and Kellog G L 2002 *J. Phys.: Condens. Matter* **14** 4227
[6] Tober E D, Farrow R F C, Marks R F, Witte G, Kalki K and Chambliss D D 1998 *Phys. Rev. Lett.* **81** 1897
[7] Tober E D, Marks R F, Chambliss D D, Roche K P, Toney M F, Kellock A J and Farrow R F C 2000 *Appl. Phys. Lett.* **77** 2728
[8] Hwang R Q 1996 *Phys. Rev. Lett.* **76** 4757
[9] Volkmann T, Much F, Biehl M and Kotrla M 2005 *Surf. Sci.* **586** 157
[10] Ozoliņš V, Asta M and Hoyt J J 2002 *Phys. Rev. Lett.* **88** 096101
[11] Ng K-O and Vanderbilt D 1995 *Phys. Rev.* B **52** 2177
[12] Kotrla M 1996 *Comput. Phys. Commun.* **97** 82–100
[13] Sabiryanov R F, Larsson M I, Cho K J, Nix W D and Clemens B M 2003 *Phys. Rev.* B **67** 125412
[14] Biehl M 2005 *Multiscale Modeling in Epitaxial Growth* vol 149, ed A Voigt (Basle: Birkhäuser) p 3
[15] Biehl M, Much F and Vey C 2005 *Multiscale Modeling in Epitaxial Growth* vol 149, ed A Voigt (Basle: Birkhäuser) p 41
[16] Schindler A 1999 *PhD Thesis* Universität Duisburg
[17] Much F, Ahr M, Biehl M and Kinzel W 2001 *Europhys. Lett.* **56** 791
[18] Much F, Ahr M, Biehl M and Kinzel W 2002 *Comput. Phys. Commun.* **147** 226
[19] Walther M, Biehl M and Kinzel W 2007 *Phys. Status Solidi* c **4** 3210–20
[20] Much F and Biehl M 2003 *Europhys. Lett.* **63** 14
[21] Schroeder M and Wolf D E 1997 *Surf. Sci.* **375** 129
[22] Jones J E 1924 *Proc. R. Soc.* A **106** 463
[23] Newman M E J and Barkema G T 1999 *Monte Carlo Methods in Statistical Physics* (Oxford: Oxford University Press)
[24] Ahr M and Biehl M 2002 *Surf. Sci.* **505** 124
[25] Zhen S and Davies G J 1983 *Phys. Status Solidi* a **78** 595
[26] Günther C, Vrijmoeth J, Hwang R Q and Behm R J 1995 *Phys. Rev. Lett.* **74** 754
[27] Van Gastel R, Plass R, Bartelt N C and Kellog G L 2003 *Phys. Rev. Lett.* **91** 55503